A Lung-Inspired Approach to Scalable and Robust Fuel Cell Design

P. Trogadas, *[a,b] J. I. S. Cho, *[a,b] T. P. Neville, [a,b] J. Marquis, [c] B. Wu, [d] D. J. L. Brett [b] and M.-O. Coppens †[a]

[a.] *EPSRC "Frontier Engineering" Centre for Nature Inspired Engineering & Department of Chemical Engineering, University College London, London WC1E 7JE, United Kingdom.*
[b.] *Electrochemical Innovation Lab, Department of Chemical Engineering, University College London, London WC1E 7JE, United Kingdom.*
[c.] *Department of Chemical and Biological Engineering, Rensselaer Polytechnic Institute, Troy, NY 12180 [current address: Momentive Performance Materials, Waterford, NY 12188*]
[d.] *Department of Mechanical Engineering, Imperial College, London SW7 2AZ, United Kingdom.*
* Both authors contributed equally.
† Corresponding author: m.coppens@ucl.ac.uk

Supplementary Information

Contents

Section S1: Theoretical model

The main modeling assumptions are the following:[1-3]

- Steady state operation
- Ideal gases
- Fully hydrated polymer electrolyte membrane
- No gas crossover
- Electronic conduction between the gas diffusion and the catalyst layer is high enough to neglect electronic resistance
- Uniform catalyst nanoparticle size and uniform Nafion® film thickness on these nanoparticles
- No liquid water present in the anode

The governing equations for a fuel cell are as follows.

S1.1 Transport of gas species within the porous media (GDL and catalyst). To evaluate the velocity and pressure profiles of the gaseous mixture inside the porous media, the continuity equation (eqn. S1) and Darcy's law (eqn. S2) are used:

$$\nabla.\left(\rho_g \cdot u_g\right) = 0 \tag{S1}$$

$$u_g = \frac{-k_p}{\mu_g} \cdot \nabla P \tag{S2}$$

where ρ_g (kg m^{-3}), u_g (m s^{-1}) and μ_g (Pa s) are the density, velocity and viscosity of the gaseous mixture, respectively, k_p (m^2) is the permeability of the porous medium and P (Pa) is the total pressure. The Stefan-Maxwell equations (eqn. S3) are used to describe the multi-component diffusion:

$$\nabla x_i = \sum_{j=1, j\neq i} \frac{1}{C \cdot D_{ij}^{eff}} \cdot \left(x_i \cdot N_j - x_j \cdot N_i\right) \tag{S3}$$

where D_{ij}^{eff} ($m^2\ s^{-1}$) is the effective binary diffusivity of species *i* in a mixture of species *i* and *j*, x_i is the mole fraction of species *i*, N_i (mol $m^{-2}\ s^{-1}$) is the molar flux of species *i*, and *C* (mol m^{-3}) is the total molar concentration of gas. Combination of eqns (S1-S3) results in:

$$\nabla \cdot \left\{ \frac{-\rho_g \cdot w_i \cdot \sum_j D_{ij}^{eff} \left[\nabla x_j + \left(x_j - w_j \right) \cdot \nabla P \right]}{P} \right\} = M_i \cdot S_i - \rho \cdot u_g \cdot \nabla w_i \qquad \text{(S4)}$$

where w_i and S_i (kg $m^{-3}\ s^{-1}$) are the mass fraction and source term of species *i*, respectively.

The Bruggeman correlation is employed to calculate the effective gas diffusion coefficient[1], which accounts for the reduction in pore space available due to the presence of liquid water in the porous medium.

$$D_{ij}^{eff} = D_{ij} \cdot \left[\varepsilon^v \cdot (1 - s) \right]^{.5} \qquad \text{(S5)}$$

where ε^v, *s* and D_{ij} ($m^2\ s^{-1}$) are the void fraction of the porous medium, saturation and binary diffusivity, respectively.

S1.2 Transport of liquid water through the GDL and catalyst layer (cathode). Liquid water transport is driven by capillary force and hence, Darcy's law (eqn. S6) is used to describe the flow of liquid inside the porous medium:[1]

$$N_w = -\frac{\rho_w}{M_w} \left[\frac{K_w(s)}{\mu_w} \cdot \nabla P_l \right] \qquad \text{(S6)}$$

where P_l (Pa), ρ_W (kg m^{-3}), K_W (m^2), M_W (g mol^{-1}) and μ_W (Pa s) are the pressure, density, permeability, molecular weight and viscosity of liquid water, respectively. Analytical equations (S7-S10) for the description of capillary pressure (P_c), permeability through the porous medium (K_W) and capillary diffusion coefficient (D_c, $m^2\ s^{-1}$) are listed below.

The capillary pressure P_c (Pa) is expressed by the following empirical correlation:[4]

$$P_c(s) = P_g - P_l = d \left[e^{-\alpha_1 (s-c)} - e^{-\alpha_2 (s-c)} \right] + b \qquad \text{(S7)}$$

where *s* is the saturation level, P_g (Pa) is the gas phase pressure and a_1, a_2, *c* and *d* are fitting parameters (Table S1).

Table S 1. Parameters for the capillary pressure correlation in the GDL and catalyst layer.[1]

Capillary function	a_1	a_2	***b* (Pa)**	***c***	***d* (Pa)**
GDL	-17.3	-25.1	32.3	0.350	-4.06
CL	-23.5	-17.4	477	0.460	-3.58

The permeability of the porous medium depends on the liquid water saturation[4], as given by eqn. (S8):

$$K_w(s) = K_{w,0} \cdot s^{4.5} \tag{S8}$$

where $K_{w,0}$ (m^2) is the permeability of liquid water at 100% saturation level.[5] Substituting eqns. (S7) and (S8) into eqn. (S6) yields the following expression for the liquid water flux:

$$N_w = -\frac{\rho_w \cdot K_{w,0}}{M_w \cdot \mu_w} \cdot s^{4.5} \cdot \nabla P_c = -D_c \cdot \frac{\rho_w}{M_w} \cdot \nabla s \tag{S9}$$

where the capillary diffusion coefficient, D_c ($m^2\ s^{-1}$), is defined as:

$$D_c = -\frac{K_{w,0}}{\mu_w} \cdot \frac{dP_c}{ds} \cdot s^{4.5} \tag{S10}$$

S1.3 Transport of dissolved water through the polymer electrolyte membrane. The dissolved water in the membrane is driven by electro-osmotic drag, diffusion and hydraulic permeation. However, since the modeled fuel cell system operates under isobaric condition, the hydraulic permeation term is neglected. Hence, the water flux in the polymer electrolyte membrane can be written as:

$$N_w^N = \frac{i_N \cdot n}{F} - D_w^N \cdot \nabla C_w^N \tag{S11}$$

where i_N ($A\ m^{-2}$) is the electrolyte current density vector, n is the electro-osmotic drag coefficient, and D_W^N ($m^2\ s^{-1}$) and C_W^N ($mol\ m^{-3}$) are the diffusivity and concentration of water in the polymer electrolyte membrane, respectively. Assuming that the polymer electrolyte membrane is fully hydrated, the concentration gradient term is neglected, and eqn. (S11) becomes:

$$\nabla . \left(\frac{i_N \cdot n}{F} \right) = 0 \tag{S12}$$

S1.4 Transport of charge & local rate of reaction in catalyst layer. Ohm's law is used to describe the ionic and electronic charge transport:

$$i_s = -\sigma_s \cdot \nabla \phi_s,\ i_N = -\sigma_N \cdot \nabla \phi_N \tag{S13}$$

where σ_s and σ_N ($S\ m^{-1}$) are the electronic and ionic conductivities, while ϕ_s and ϕ_N (V) are the solid and electrolyte phase potentials, respectively. The charge balance equations (S13) are solved to obtain electrolyte and solid phase potentials:

$$\nabla . (-\sigma_N \cdot \nabla \phi_N) = S_\phi \tag{S14}$$

$$\nabla . (-\sigma_s \cdot \nabla \phi_s) = -S_\phi \tag{S15}$$

In the catalyst layer, the source term S_ϕ represents the local rate of reaction. S_ϕ is zero in the polymer electrolyte membrane and GDL as no reactions take place in these domains.

S1.5 Local rate of reaction in the catalyst layer. Assuming that the catalyst layer consists of individual spherical catalyst agglomerates, the oxygen reduction reaction rate (mol m^{-3} s^{-1}) is equal to:[6]

$$R_{O_2} = \left[\frac{\frac{R \cdot T}{H_{O_2}}}{\frac{\delta_N \cdot (\delta_N + r_{agg})}{r_{agg} \cdot \alpha_r \cdot D_{O_2}^N} + \frac{\delta_w \cdot (\delta_w + \delta_N + r_{agg})}{(\delta_N + r_{agg}) \cdot \alpha_r \cdot D_{O_2}^w} + \frac{1}{\xi \cdot k_t}} \right] C_{O_2} \tag{S16}$$

where R (8.314 J mol^{-1} K^{-1}) is the universal gas constant, H_{O2} (atm m^3 mol^{-1}) is Henry's constant of oxygen between air and electrolyte, δ_N and δ_W (m) are the ionomer and water film thicknesses surrounding the catalyst agglomerate, r_{agg} (m) is the catalyst agglomerate radius, $D_{O_2}^N$ and $D_{O_2}^w$ (m^2 s^{-1}) are the diffusivity of oxygen in ionomer film and water, respectively, a_r (m^2 m^{-3}) is the effective agglomerate surface area, ξ is the agglomerate effectiveness factor, and k_t (s^{-1}) is the reaction rate constant.

The effectiveness factor, ξ, for a spherical catalyst agglomerate in eqn. (S16) is given by:

$$\xi = \frac{1}{\varphi} \cdot \frac{3 \cdot \varphi \cdot \coth(3 \cdot \varphi) - 1}{3 \cdot \varphi} \tag{S17}$$

where the Thiele modulus, φ, is equal to:[6]

$$\varphi = \frac{r_{agg}}{3} \cdot \sqrt{\frac{k_t}{(1 - \varepsilon_v^{cl}) D_{O_2,eff}^N}} \tag{S18}$$

The Bruggeman correlation is used to describe the effective oxygen diffusivity inside the agglomerate:

$$D_{O_2,eff}^N = D_{O_2}^N \cdot \frac{\varepsilon_N^{agg}}{\tau_{agg}} \tag{S19}$$

and the reaction rate constant k_t is expressed by:

$$k_t = (1 - \varepsilon_v^{cl}) \frac{\alpha_{Pt}^{agg} \cdot i_{0,c}}{4 \cdot F \cdot C_{O_2}^{ref}} \cdot \exp\left[\frac{-\alpha_c \cdot F}{R \cdot T} \cdot (V_A - \phi_m - U_{eq}) \right] \tag{S20}$$

where ε_v^{cl} (m) is the porosity of the catalyst layer, $i_{0,c}$ (A m^{-2}) is the reference exchange current density for the cathode, $C_{O_2}^{ref}$ (mol m^{-3}) is the reference oxygen concentration in the catalyst layer, α_c is the cathodic transfer coefficient, V_A (V) is the applied cell voltage, U_{eq} (V) is the standard equilibrium potential of the oxygen reduction reaction and ϕ_m (V) is the overpotential.

The effect of the catalyst morphology is considered via the utilization of active catalyst surface area per unit volume of agglomerates, a_{Pt}^{agg} (m^2 m^{-3}), which is defined as:

$$\alpha_{Pt}^{agg} = \frac{\alpha_{Pt} \cdot m_{Pt}}{t_{cl} \cdot \left(1 - \varepsilon_v^{cl}\right)} \tag{S21}$$

where m_{pt} (g_{Pt} m^{-2}) is the platinum loading, t_{cl} (m) is the catalyst layer thickness, and a_{pt} (m^2 g^{-1}) is the surface area per unit mass of platinum particle, which is estimated from an empirical correlation for a supported platinum catalyst:[2]

$$\alpha_{Pt} = 2.2779 \cdot 10^6 \cdot (Pt \mid C)^3 - 1.5857 \cdot 10^6 \cdot (Pt \mid C)^2 - 2.0153 \cdot 10^6 \cdot (Pt \mid C) + 1.5950 \cdot 10^6 \tag{S22}$$

where Pt|C is the mass percentage of platinum on carbon.

Liquid water forms a film on the top of Nafion® and its thickness can be estimated by:

$$\delta_w = \frac{\varepsilon_v^{cl} \cdot s}{\alpha_r} \tag{S23}$$

The effective agglomerate surface area, a_r (m^2 m^{-3}), is defined as the outer surface area of the agglomerate per unit volume of the catalyst layer and it is given by:

$$\alpha_r = \frac{3}{r_{agg} \cdot \left(1 - \varepsilon_v^{cl}\right)} \tag{S24}$$

where r_{agg} (m) is the catalyst agglomerate radius. The effectiveness factor of the hydrogen oxidation reaction (HOR) is set to 1.0, because hydrogen dissolves rapidly into the electrolyte, and the Butler-Volmer eqn. is employed to describe HOR kinetics:[7]

$$R_{H_2} = \alpha_{Pt}^{agg} \cdot i_{0,a} \cdot \left(\frac{P_{H_2}}{C_{H_2}^{ref} \cdot H_{H_2}}\right)^{0.5} \left[\exp\left(\frac{-(1-\alpha_a) \cdot F \cdot \eta_a}{R \cdot T}\right) - \exp\left(\frac{\alpha_a \cdot F \cdot \eta_a}{R \cdot T}\right)\right] \tag{S25}$$

where $i_{0,a}$ (A m^{-2}) is the reference exchange current density for the anode, P_{H2} (Pa) is the partial pressure of hydrogen, $C_{H_2}^{ref}$ (mol m^{-3}) is the reference oxygen concentration in the catalyst layer, H_{H2} (atm m^3 mol^{-1}) is Henry's constant of hydrogen between air and electrolyte, α_a is the anodic transfer coefficient, and η_a (V) is the anodic overpotential.

S1.6 Water phase change. The rate of water phase change (mol m^3 s^{-1}) in the porous media is expressed by:[1]

$$S_{phase}=\begin{cases} k_c \cdot \dfrac{\varepsilon_i^v \cdot (1-s)\cdot y_v}{R\cdot T}\cdot\left(y_v \cdot P - P_v^{sat}\right) & y_v \cdot P \geq P_v^{sat} \\ k_v \cdot \dfrac{\varepsilon_i^v \cdot s \cdot \rho_w}{M_w}\cdot\left(y_v \cdot P - P_v^{sat}\right) & y_v \cdot P < P_v^{sat} \end{cases} \quad \text{(S26)}$$

where y_v is the mole fraction of liquid water, ρ_w (kg m^{-3}) is the density of liquid water, M_w (g mol^{-1}) is the molecular weight of water, P (Pa) is the total pressure, k_c and k_v (s^{-1}) are the condensation and evaporation rate constants, respectively. The vapor saturation pressure, P_v^{sat} (Pa), is calculated via the Antoine equation:[8]

$$P_v^{sat} = \exp\left[16.3872 - \frac{3885.7}{(T-273.15)+230.17}\right] \quad \text{(S27)}$$

S1.7 Parameter values. A list of detailed parameter values used in the lung-inspired fractal flow field based PEFC model is presented in Table S2.

Table S 2. Parameter values used in the lung-inspired flow field based PEFC model.

Geometry	Value	Units	Source	Parameter	Value	Units	Source
A	10^{-3}	m^2		t_{GDL}	350×10^{-6}	m	[9]
r_{agg}	150×10^{-9}	m	[6]	t_{CL}	40×10^{-6}	m	[10]
$W_{c,1}$	0.25×10^{-2}	m		t_{mem}	150×10^{-6}	m	[11]
Operating conditions							
P	1.1	atm	[12]	x_{O2}	0.11	-	[6]
T	353	K	[2]	x_{N2}	0.42	-	[6]
$S_{Cathode}$	2.0		[13]	x_w	0.47	-	[6]
S_{Anode}	2.0	-	[14]	U_{ref}	1.0	V	[1]
Physical properties							
$C_{O2,ref}$	0.85	mol m^{-3}	[2]	$i_{0,c,273}$	1.0×10^{10}	A m^{-2}	[1]
$C_{H2,ref}$	5.64×10^{-11}	mol m^{-3}	[15]	$i_{0,c}$	$i_{0,273} \times 2^{(T-273)/10} \times 10^{-4}$	A m^{-2}	[16]
α_c	1.0	-	[13]	$i_{0,a}$	1×10^{-4}	A m^{-2}	[17]
α_a	0.5	-	[3]	μ_w	3.5×10^{-4}	Pa s	[18]
H_{H2}	4.5×10^{-2}	atmm^{3}mol^{-1}	[15]	ρ_C	2.0×10^{-6}	g m^{-3}	[2]
H_{O2}	3.56×10^{4}	atmm^{3}mol^{-1}	[19]	ρ_{Pt}	21.5×10^{-6}	g m^{-3}	[2]
n	0.11 x λ	-	[20]	$\varepsilon_{V,GDL}$	0.75	-	[21]
λ	$C_{W,N} / C_f$	-	[1]	$\varepsilon_{V,CL}$	0.5	-	[6]
$C_{W,N}$	4.2×10^{-3}	mol m^{-3}	[1]	$\varepsilon_{agg,N}$	0.66	-	[6]
C_f	1.2×10^{-3}	mol m^{-3}	[1]	m_{pt}	0.4×10^{-4}	mg m^{-2}	[6]
k_v	100	atm^{-1} s^{-1}	[1]	k_c	100	s^{-1}	[1]
Pt|C	0.28	-	[6]				
Transport properties							
$D_{O2,H2O}$	$2.82 \times 10^{-5} \times (T/308.1)^{1.5}$	m^2 s^{-1}	[22]	$k_{p,CL}$	2×10^{-15}	m^2	[13]
$D_{O2,N2}$	$2.2 \times 10^{-5} \times (T/293.2)^{1.5}$	m^2 s^{-1}	[22]	$k_{p,GDL}$	2×10^{-15}	m^2	[13]
$D_{N2,H2O}$	$2.56 \times 10^{-5} \times (T/307.5)^{1.5}$	m^2 s^{-1}	[22]	$K_{w,0\text{-}GDL}$	2.0×10^{-15}	m^2	[1]
$D_{H2,H2O}$	$9.15 \times 10^{-5} \times (T/307.5)^{1.5}$	m^2 s^{-1}	[22]	$K_{w,0\text{-}CL}$	5.0×10^{-17}	m^2	[1]
$D_{O2,N}$	8.45×10^{-10}	m^2 s^{-1}	[2]	σ_m	8.9	S m^{-1}	[6]
$D_{O2,w}$	4.73×10^{-9}	m^2 s^{-1}	[6]	σ_s	1000	S m^{-1}	[23]

S1.8 Incorporation of fractal flow field design into the model. The fractal flow fields consist of self-similar, repeatedly branching "H"-shaped channels uniformly distributing reactant across the surface of the catalyst layer. The distributor has a single inlet and 4^N outlets, where N is the number of fractal generations. The fractal dimension D is expressed by:[24]

$$D = \frac{\log(n)}{\log\left(\frac{1}{s}\right)} = \frac{\log(4)}{\log(2)} = 2 \tag{S28}$$

where n is the number of daughter shapes per parent, and s is the contraction ratio between daughter and parent. A fractal dimension of 2 indicates that, given an infinite number of generations, the structure will become plane-filling. The use of this geometry allows a single inlet to branch into 4^N outlets with each flow path of equal length, allowing gas to be uniformly distributed over a planar surface (Scheme S1).

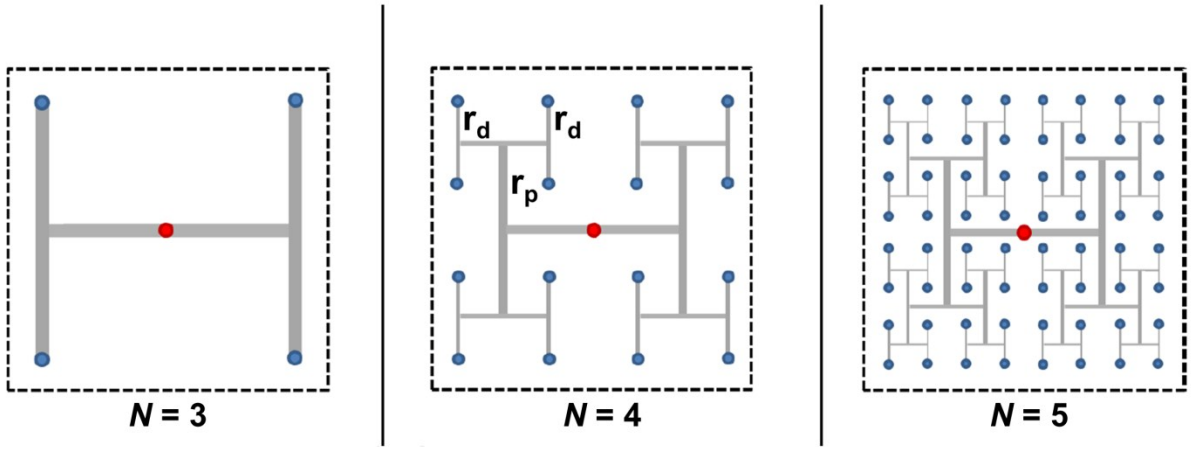

Scheme S 1. Fractal structures of different generations N for gas distribution networks in PEFCs. Red and blue dots represent fluid inlet and outlet, respectively, while dashed boxes represent active membrane area. Each H shape represents 4 daughter branches of radius r_d; the radius of each branch in an H shape is the same including the horizontal channel.

The channel width of these flow fields obeys Murray's law,which dictates the relationship between the hydraulic diameters of parent (radius r_p, m) and daughter (radius r_d, m) branches.[25]

$$r_p^3 = \sum_{i=1}^{n} r_{d_i}^3 \tag{S29}$$

By obeying Murray's law, the scaling of the channel diameters reduces the flow velocity at each generation due to a net increase in total cross-sectional area. Thus, a reduced pressure drop over each generation in the network is achieved. Given enough generations, the convective flux at the distributor outlet will match the diffusive flux at the GDL interface. This parallels the gas flow transition between the bronchial tree and the alveoli in the lung, where gas transport has been shown to be thermodynamically optimal.[26]

The dimensionless Péclet number (eqn. S30) is used to quantify the ratio of convective and diffusive fluxes:

$$Pe = \frac{L \cdot U}{D} \tag{S30}$$

where L (m) is the thickness of the catalyst layer, U (m s^{-1}) is the flow velocity, and D (m^2 s^{-1}) is the diffusivity. The flow velocity at the flow field / GDL interface is described by:

$$U = \frac{Q_0}{A_N \cdot 4^N} \tag{S31}$$

where Q_O (m^3 s^{-1}) is the volumetric flow rate of gas at the inlet, and A_N (m^2) is the cross-sectional area of a single outlet of the N^{th} generation.

S1.9 Boundary conditions (BCs)

BC at the anode gas channel / anode GDL interface:

$$C_{H_2}^{g} = C_{H_2}^{in} \tag{S32}$$

BCs at the cathode gas channel / cathode GDL interface:

$$C_{O_2}^{g} = C_{O_2}^{air} \tag{S33}$$

$$C_{v}^{g} = C_{v}^{g,air} \tag{S34}$$

BCs at the anode GDL / anode catalyst layer (ACL) interface:

$$N_{H_2}^{g} \mid_{GDL} = N_{H_2}^{g} \mid_{ACL} \tag{S35}$$

$$i_N \mid_{ACL} = 0 \tag{S36}$$

BCs at the cathode GDL / cathode catalyst layer (CCL) interface:

$$N_{O_2}^{g} \mid_{GDL} = N_{O_2}^{g} \mid_{CCL} \tag{S37}$$

$$N_{N_2}^{g} \mid_{GDL} = N_{N_2}^{g} \mid_{CCL} \tag{S38}$$

$$N_{v}^{g} \mid_{GDL} = N_{v}^{g} \mid_{CCL} \tag{S39}$$

$$i_N \mid_{CCL} = 0 \tag{S40}$$

$$P_c \mid_{GDL} = P_c \mid_{CCL} \tag{S41}$$

BCs at the ACL / polymer electrolyte membrane (MEM) interface:

$$N_{H_2}^{g} \mid_{ACL} = 0 \tag{S42}$$

$$i_N \mid_{ACL} = i_N \mid_{MEM} \tag{S43}$$

$$C_{H_2}^{g} = 0 \tag{S44}$$

$$\Phi_N = 0 \tag{S45}$$

BCs at the CCL / MEM interface:

$$N_{O_2}^{g} \mid_{CCL} = 0 \tag{S46}$$

$$N_{w}^{g} \mid_{CCL} = 0 \tag{S47}$$

$$i_N \mid_{CCL} = i_N \mid_{MEM} \tag{S48}$$

$$N_w \mid_{CCL} = N_w^N \mid_{MEM} \tag{S49}$$

$$C_{O_2}^{g} = 0 \tag{S50}$$

$$C_{v}^{g} = 0 \tag{S51}$$

$$C_{N_2}^{g} = 0 \tag{S52}$$

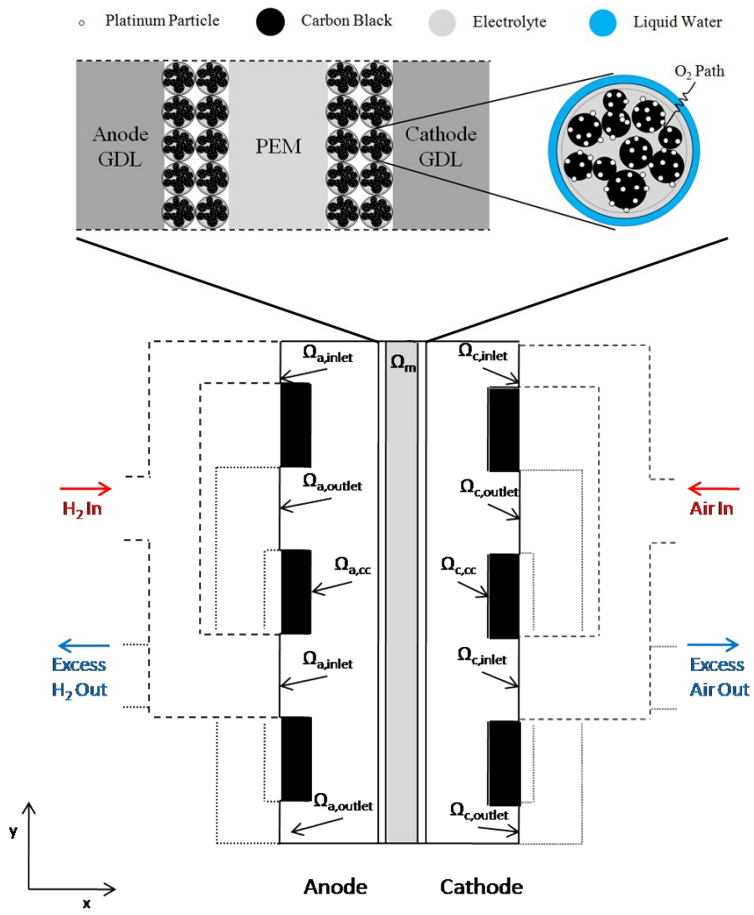

Figure S 1. Modeling domain of the lung-inspired flow field based PEFC.[27]

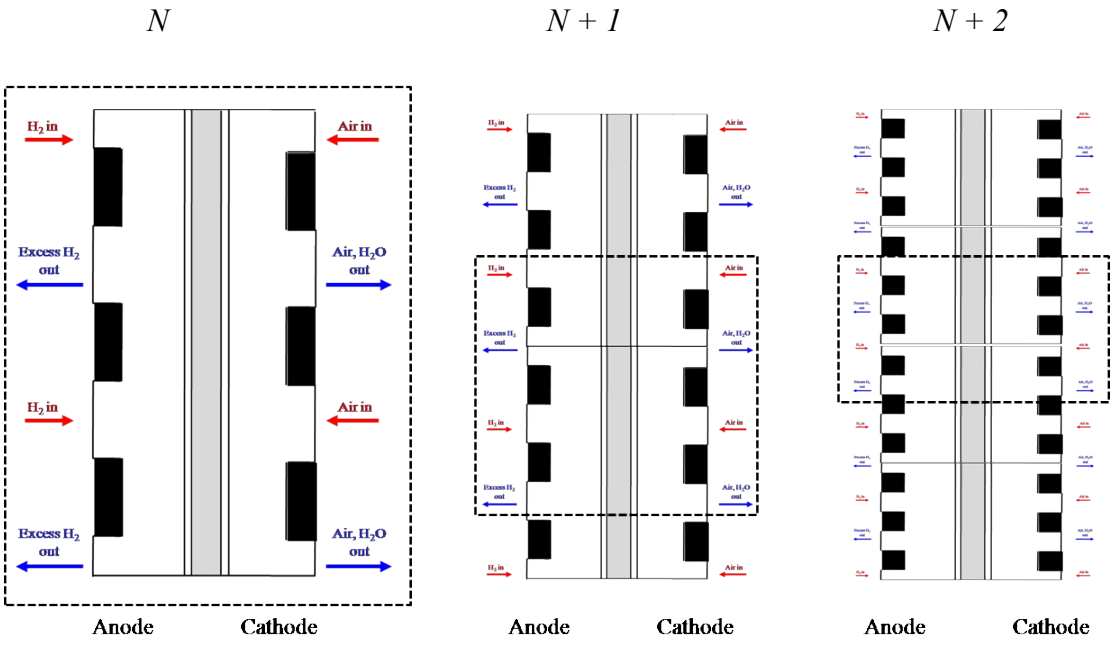

Figure S 2. Schematic representation of the modeling domain of lung-inspired flow field based PEFC at various fractal generations. The rectangular box shows what is actually being modeled.[27]

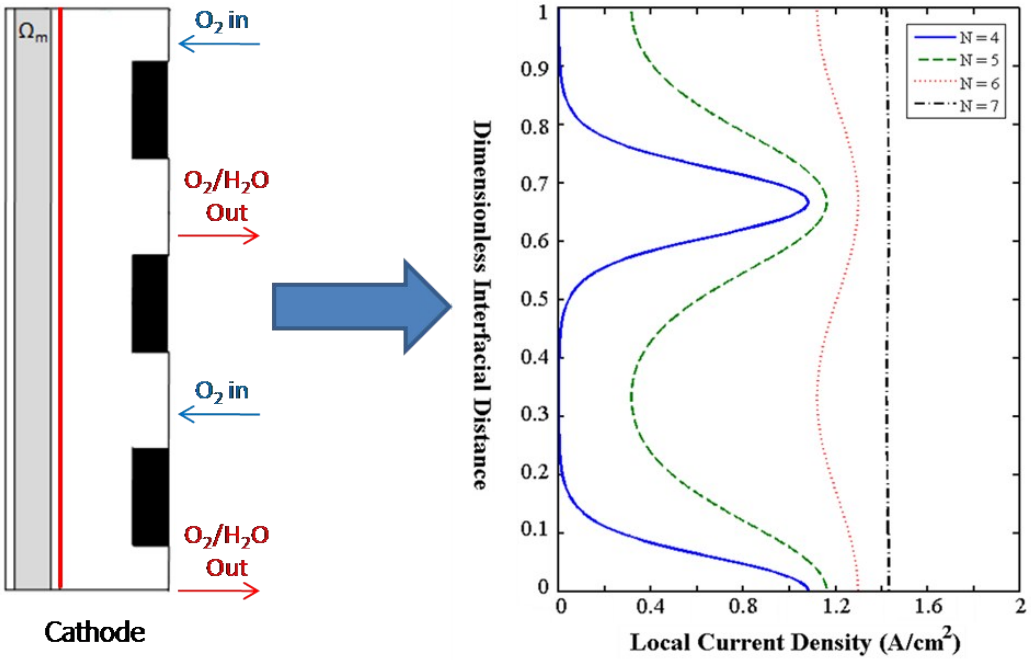

Figure S 3. Simulation results showing the effect of the number of branching generations on the distribution of the current density across the electrode.

Section S2: Experimental details

S2.1 Fractal flow-field design. The inlet and outlet channel geometries of each fractal flow-field are outlined in Table S3.

Table S 3. Fractal flow field inlet and outlet channel geometries.

Number of generations	Inlet channel dimension (mm)	Number of outlet channels	Outlet channel dimension (mm)	Distance between outlets (mm)
3	2.16 × 2.16	64	0.7 × 0.8	3.85
4	0.74 × 0.97	256	0.5 × 0.75	1.93
5	0.30 × 0.60	1024	0.3 × 0.5	1.20

S2.2 Manufacturing of fractal flow fields for the cathode side. The fractal prototype with N = 3 (Concept Laser GmbH, Germany), N = 4 and N = 5 (FineLine Prototyping, USA) generations were 3D printed in stainless steel via Direct Metal Laser Sintering (DMLS). The prototypes were designed using Siemens NX 7.5 (Siemens PLM Software, Germany) or Rhino 4.0 (Robert McNeel & Associates, USA) software and the designs were rendered to .stl files before being discretised into thin layers to be printed. The prototypes were printed through a repeated process of stainless steel powder layering, followed by selective laser sintering, in locations defined by the 2D slice data. A temporary support structure was included to maintain the structural integrity during the build.

X-ray radiography was used for the structural evaluation of the flow fields. Scans were carried out using an Xradia Versa 520 (Zeiss instrument, Germany). The samples were

mounted on to the sample holder and imaged at 16 kV with a pixel size of 33 x 33 μm and beam power of 10W.

All fractal flow-field prototypes were tested against a single and double serpentine flow-field with channel width, land and depth of 1 mm.

S2.3 Gold electroplating of fractal flow fields. Prior to gold electrodeposition, all 3D printed flow fields were cleaned with acetone, followed by sonication in DI water for 1 minute. These flow fields were then immersed into 0.02 M gold potassium cyanide solution ($KAu(CN)_2$) and a titanium coated stainless steel mesh was used as counter electrode. The electroplating solution was continuously stirred at 100 rpm to minimize local variation in gold concentration throughout the electroplating process. A Gamry potentiostat (Reference 3000) was used to hold the current density at 10 $mAcm^{-2}$ for 525 s to electroplate 1 μm of gold onto the 3D printed flow fields. The fractal flow field with N = 3 generations had a submerged surface area of 38 cm^2 ($I_{electrodeposition}$ = 380 mA), while the fractal flow fields with N = 4 and 5 generations had a submerged surface area of 30 cm^2 ($I_{electrodeposition}$ = 300 mA) each. After electroplating of each flow field, the concentration of the solution was adjusted by adding 0.08 M $KAu(CN)_2$ gold replenisher solution, and the electroplating process continued for the next fractal flow field.

S2.4 Membrane electrode assembly (MEA) fabrication. 10 and 25 cm^2 MEAs were fabricated in-house by hot pressing Nafion® HP membrane (DuPont, USA) and ELE0201 gas diffusion electrodes (Johnson Matthey, UK) using a 12-ton thermal press (Carver, 4122CE). The membrane was used without any pre-treatment and the MEA was pressed at 130°C for 4 minutes with an applied pressure of 400 psi.

S2.5 PEFC operation. Fuel cell temperature, inlet gas flow rate and relative humidity were regulated using an 850e fuel cell station (Scribner Associates, USA). The stoichiometry of anode and cathode were kept constant at 1.2 and 3, respectively, and total loading was 0.4 $mg_{Pt}\,cm^{-2}$. The inlet gas relative humidity of the anode was kept the same as the cathode and the cell temperature was set to 70°C. The outlet of both the anode and cathode was at atmospheric pressure.

Extended current hold measurements (24 h) were conducted using the same operating conditions as detailed above.

Section S3: Additional figures

S3.1 PEFC performance at 100%RH (10 and 25 cm^2 flow field area)

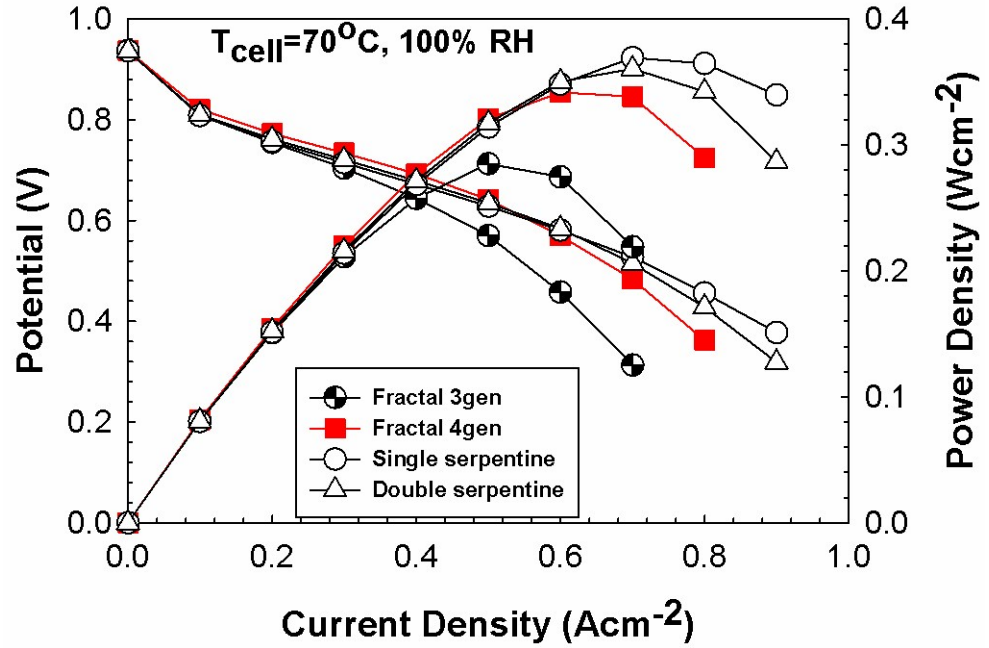

Figure S 4. Polarization and power density curves at 100%RH for fractal and serpentine flow-field (10 cm^2 surface area) based PEFCs.

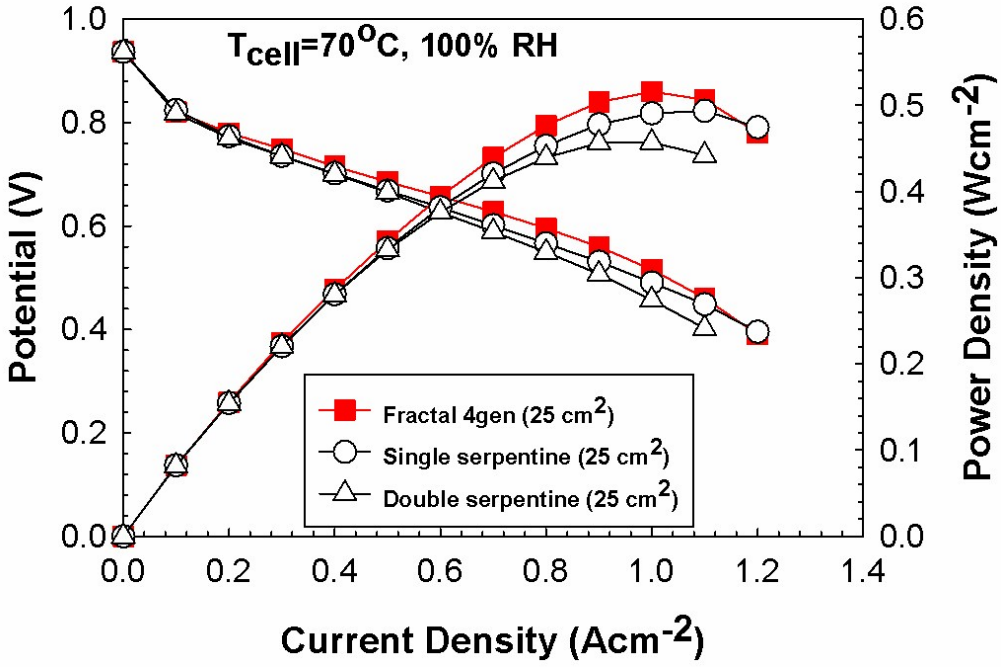

Figure S 5. Polarization and power density curves at 100%RH for fractal and serpentine flow-field (25 cm^2 surface area) based PEFCs.

S3.2 Pressure drop (10 cm^2 flow field area)

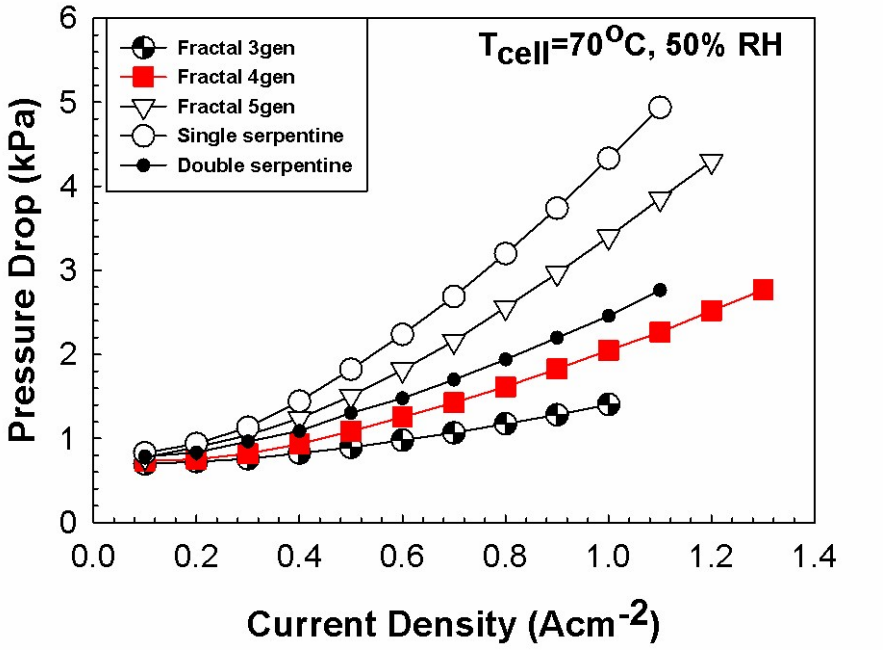

Figure S 6. Pressure drop in the cathode for fractal and serpentine flow-field (10 cm^2 surface area) based PEFCs at 50% RH.

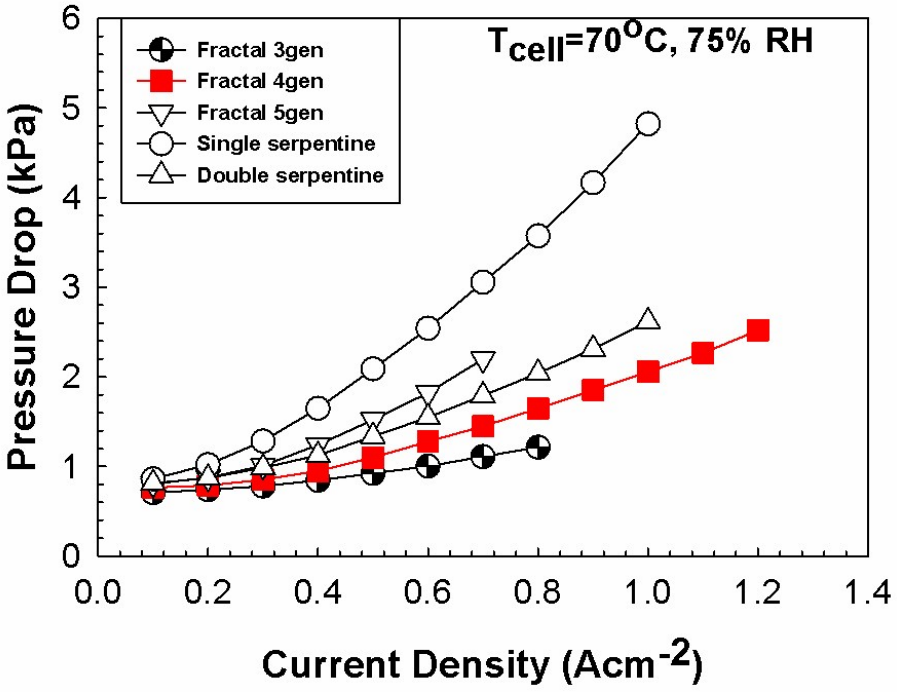

Figure S 7. Pressure drop in the cathode for fractal and serpentine flow-field (10 cm^2 surface area) based PEFCs at 75% RH.

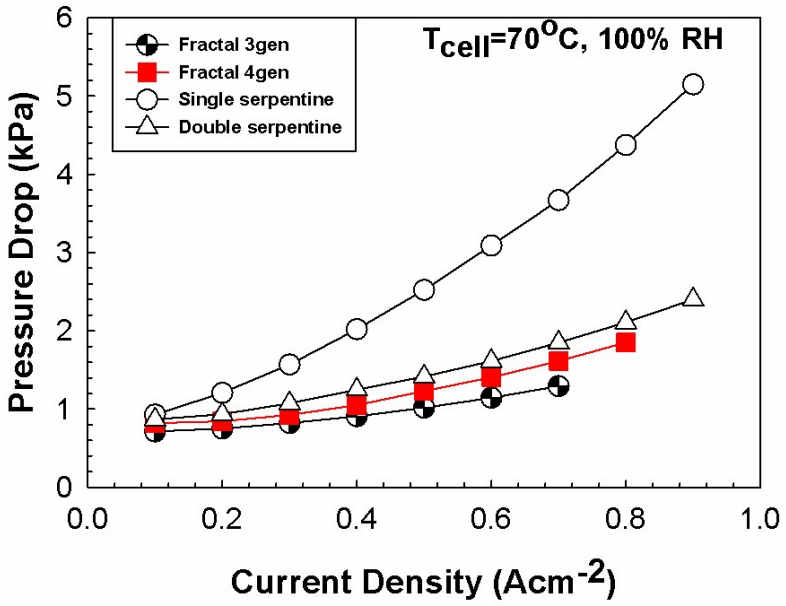

Figure S 8. Pressure drop in the cathode for fractal and serpentine flow-field (10 cm^2 surface area) based PEFCs at 100% RH.

S3.3 Pressure drop (25 cm^2 flow field area)

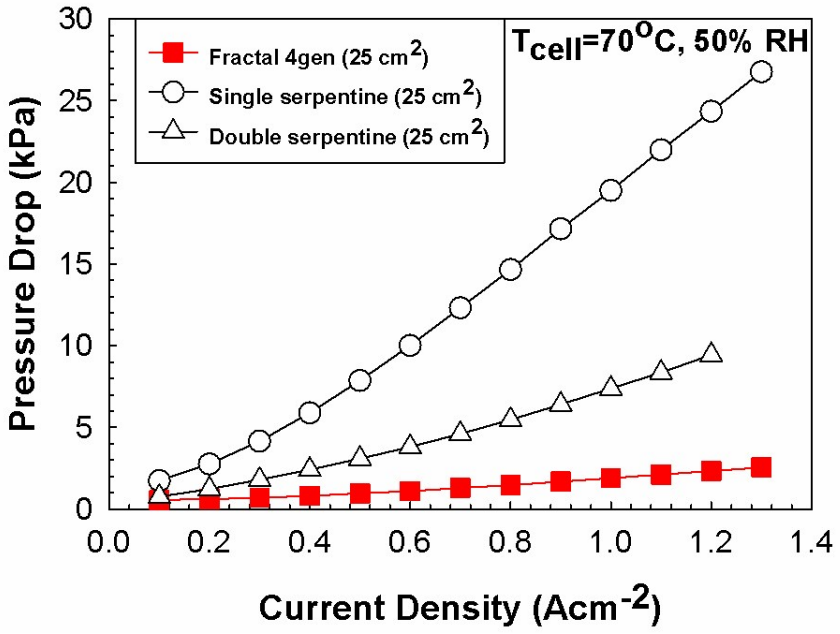

Figure S 9. Pressure drop in the cathode for fractal and serpentine flow-field (25 cm^2 surface area) based PEFCs at 50% RH.

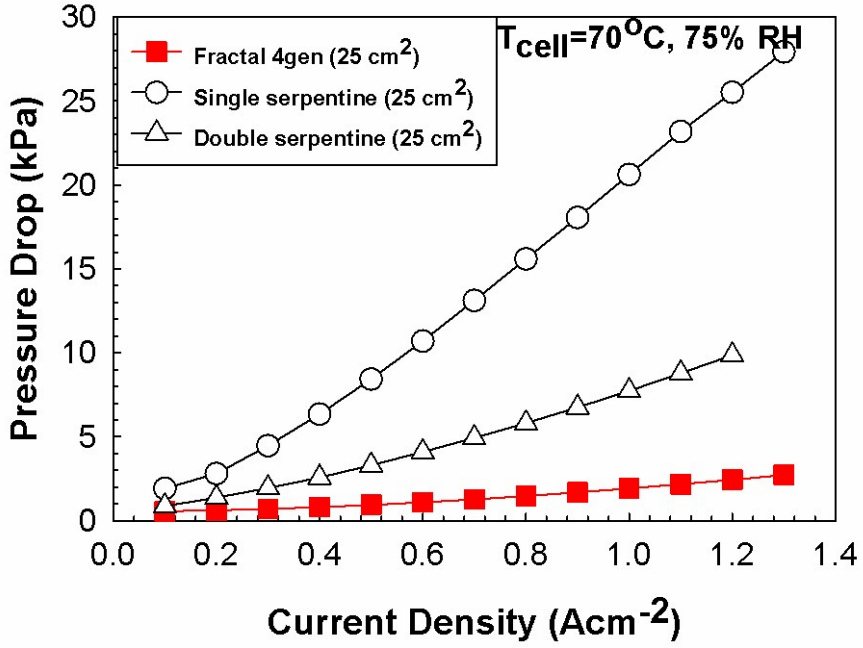

Figure S 10. Pressure drop in the cathode for fractal and serpentine flow-field (25 cm^2 surface area) based PEFCs at 75% RH.

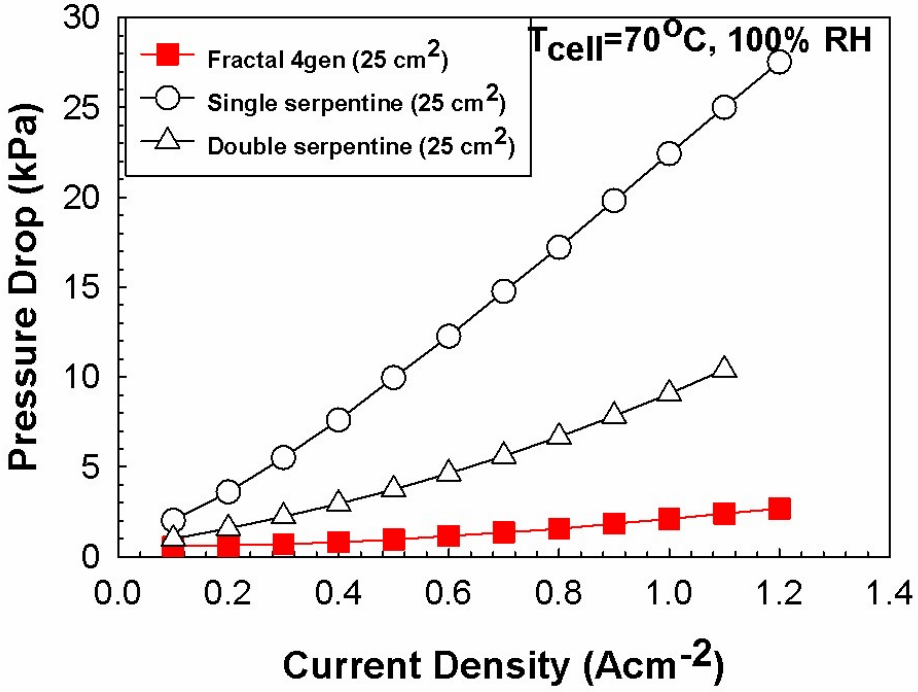

Figure S 11. Pressure drop in the cathode for fractal and serpentine flow-field (25 cm^2 surface area) based PEFCs at 100% RH.

S3.4 High frequency resistance (10 cm^2 flow field area)

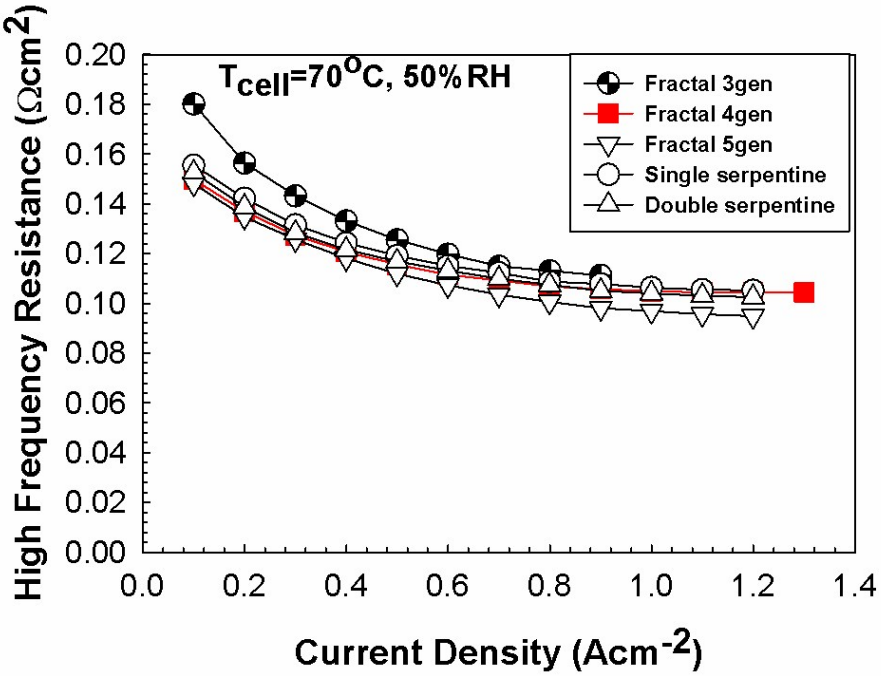

Figure S 12. High frequency resistance values at 50%RH for fractal with N = 3, 4, 5 and conventional serpentine flow-field based PEFCs.

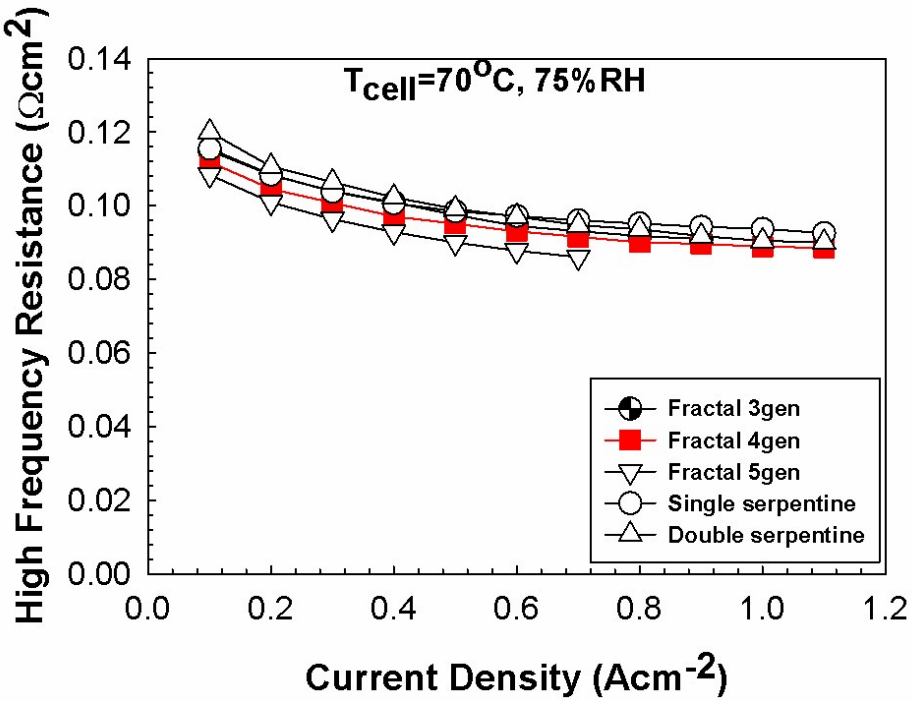

Figure S 13. High frequency resistance values at 75%RH for fractal with N = 3, 4, 5 and conventional serpentine flow-field based PEFCs. Single and double serpentine high frequency resistance values overlap fractal 3gen values.

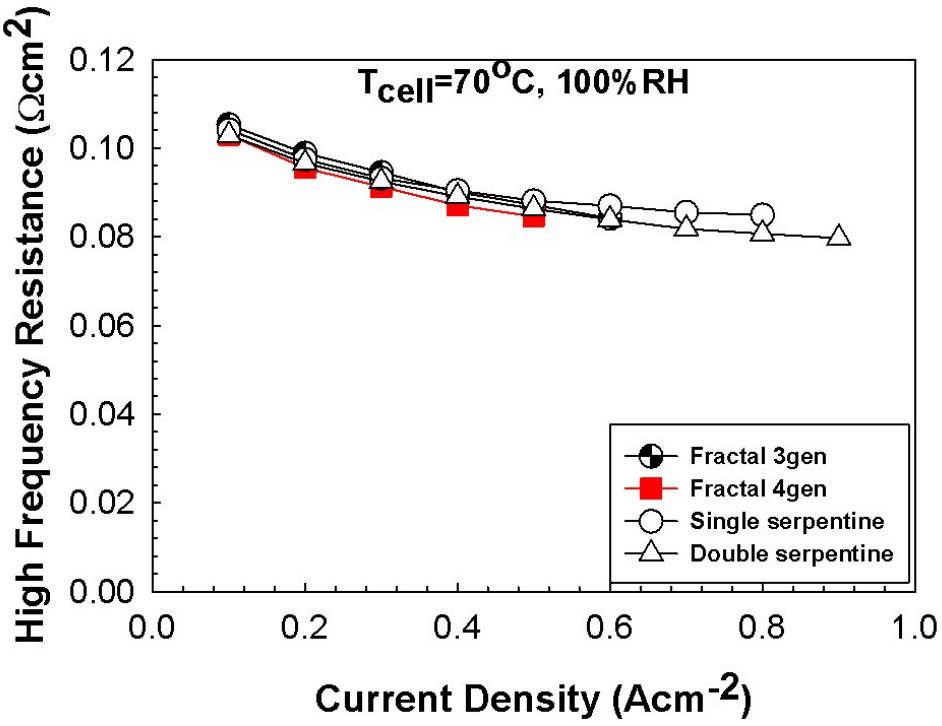

Figure S 14. High frequency resistance values at 100%RH for fractal with N = 3, 4, 5 and conventional serpentine flow-field based PEFCs.

References

1. X. Wang and T. Van Nguyen, *Journal of the Electrochemical Society*, 2008, **155**, B1085-B1092.
2. M. Secanell, K. Karan, A. Suleman and N. Djilali, *Electrochimica Acta*, 2007, **52**, 6318-6337.
3. W. Sun, B. A. Peppley and K. Karan, *Electrochimica Acta*, 2005, **50**, 3359-3374.
4. Q. Ye and T. Van Nguyen, *Journal of the Electrochemical Society*, 2007, **154**, B1242-B1251.
5. D. Natarajan and T. Van Nguyen, *Journal of Power Sources*, 2003, **115**, 66-80.
6. J. Marquis and M.-O. Coppens, *Chemical Engineering Science*, 2013, **102**, 151-162.
7. F. Barbir, *PEM Fuel Cells: Theory and Practice*, Academic Press, 2012.
8. J. M. Smith, H. C. Van Ness and M. M. Abbott, *Introduction to Chemical Engineering Thermodynamics*, McGraw-Hill, Boston, 7th edn., 2005.
9. M. Mortazavi and K. Tajiri, *ASME 2013 11th International Conference on Fuel Cell Science, Engineering and Technology*, 2013, DOI: 10.1115/FuelCell2013-18361, V001T001A016.
10. A. Z. Weber and J. Newman, *Journal of the Electrochemical Society*, 2007, **154**, B405-B412.
11. V. O. Mittal, H. R. Kunz and J. M. Fenton, *Journal of The Electrochemical Society*, 2007, **154**, B652-B656.
12. B. Zhou, W. Huang, Y. Zong and A. Sobiesiak, *Journal of Power Sources*, 2006, **155**, 190-202.
13. A. Z. Weber, R. M. Darling and J. Newman, *Journal of the Electrochemical Society*, 2004, **151**, A1715-A1727.
14. S. Qu, X. Li, M. Hou, Z. Shao and B. Yi, *Journal of Power Sources*, 2008, **185**, 302-310.
15. D. M. Bernardi and M. W. Verbrugge, *Journal of the Electrochemical Society*, 1992, **139**, 2477-2491.
16. U. Pasaogullari and C.-Y. Wang, *Journal of The Electrochemical Society*, 2005, **152**, A380-A390.
17. C. Marr and X. Li, *Journal of Power Sources*, 1999, **77**, 17-27.
18. Y. Wang and X. Feng, *Journal of The Electrochemical Society*, 2008, **155**, B1289-B1295.
19. R. Sander, *Compilation of Henry's law constants for inorganic and organic species of potential importance in environmental chemistry*, Max-Planck Institute of Chemistry, Air Chemistry Department Mainz, Germany, 1999.
20. T. E. Springer, T. Zawodzinski and S. Gottesfeld, *Journal of the Electrochemical Society*, 1991, **138**, 2334-2342.
21. T. Berning, M. Odgaard and S. K. Kær, *Journal of Power Sources*, 2011, **196**, 6305-6317.
22. E. L. Cussler, *Diffusion: Mass Transfer in Fluid Systems*, Cambridge University Press, 3rd edn., 2009.
23. D. Bevers, M. WO, K. Yasuda and K. Oguro, *Journal of Applied Electrochemistry*, 1997, **27**, 1254-1264.
24. B. B. Mandelbrot, *The Fractal Geometry of Nature*, Freeman, San Francisco, 1982.
25. C. D. Murray, *Proceedings of the National Academy of Sciences of the United States of America*, 1926, **12**, 207-214.
26. S. Gheorghiu, S. Kjelstrup, P. Pfeifer and M.-O. Coppens, in *Fractals in Biology and Medicine*, Springer, 2005, pp. 31-42.
27. J. Marquis, *PhD thesis, Rensselaer Polytechnic Institute, Troy, NY*, 2013.

Nomenclature

A	active area, m^2
A_N	cross-sectional area of a single outlet at the N^{th} generation, m^2
a_r	effective agglomerate surface area, $m^2\ m^{-3}$
a_{pt}	effective catalyst surface area, $m^2\ g^{-1}$
α_{Pt}^{agg}	specific catalyst surface area, $m^2\ m^{-3}$
C	total gas concentration, $mol\ m^{-3}$
C_f	fixed charge site concentration in membrane, $mol\ m^{-3}$
C_{H2}^{ref}	reference concentration of hydrogen, $mol\ m^{-3}$
C_{O2}	concentration of oxygen in catalyst layer, $mol\ m^{-3}$
C_{O2}^{ref}	reference concentration of oxygen, $mol\ m^{-3}$
C_{O2}^{air}	concentration of oxygen in inlet air, $mol\ m^{-3}$
C_v^g	concentration of vapor, $mol\ m^{-3}$
$C_v^{g,air}$	concentration of water vapor in inlet air, $mol\ m^{-3}$
C_w^N	water concentration in membrane, $mol\ m^{-3}$
D	fractal dimension
D_c	capillary diffusion coefficient, $m^2\ s^{-1}$
D_{ij}	element of the Maxwell-Stefan diffusion coefficient matrix, $m^2\ s^{-1}$
D_{O2}^N	oxygen diffusivity in Nafion®, $m^2\ s^{-1}$
$D_{O2,N}^{eff}$	effective oxygen diffusivity in Nafion®, $m^2\ s^{-1}$
D_{O2}^w	oxygen diffusivity in water, $m^2\ s^{-1}$
D_w^N	diffusivity of water in Nafion®, $m^2\ s^{-1}$
F	Faraday's constant, 96500 $C\ mol^{-1}$
H	Henry's constant, $atm\ m^3\ mol^{-1}$

i_N	electrolyte current density, A m^{-2}
i_d	current density, A m^{-2}
i_s	electronic current density, A m^{-2}
i_0	exchange current density, A m^{-2}
k_c	condensation rate constant, s^{-1}
k_p	electrode permeability, m^2
k_v	evaporation rate constant, atm^{-1} s^{-1}
k_t	reaction rate constant, s^{-1}
K_w	water permeability, m^2
$K_{w,0}$	water permeability at 100% saturation, m^2
m_{pt}	platinum loading per unit area of catalyst layer, g_{Pt} m^{-2}
M_i	molecular weight, g mol^{-1}
n	electro-osmotic drag coefficient
N_i^g	flux of gaseous species *i*, mol m^{-2} s^{-1}
N_v^g	flux of vapor, mol m^{-2} s^{-1}
N_w	flux of liquid water, mol m^{-2} s^{-1}
N_w^g	flux of water vapor, mol m^{-2} s^{-1}
N_w^N	flux of liquid water in membrane, mol m^{-2} s^{-1}
P	total pressure, Pa
P_i	partial pressure, Pa
P_c	capillary pressure, Pa
P_l	liquid pressure, Pa
P_g	gas pressure, Pa
P^{sat}	saturation pressure, Pa
$Pt\|C$	mass percentage of platinum catalyst on carbon black, kg Pt / (kg C + kg Pt)
Q_o	volumetric flow rate of gas at the inlet, m^3 s^{-1}

r_{agg}	agglomerate radius, m
R	ideal gas constant, 8.314 J mol^{-1} K^{-1}
R_i	reaction rate, mol m^{-3} s^{-1}
S_{phase}	evaporation/condensation rate, mol m^{-3} s^{-1}
S_{Anode}	anode stoichiometry ratio, 1.2
$S_{Cathode}$	cathode stoichiometry ratio, 3
s	liquid water saturation
S	source term
T	Temperature, K
t_{CL}	catalyst layer thickness, m
t_{GDL}	gas diffusion layer thickness, m
t_{mem}	membrane thickness, m
u_g	gas phase velocity, m s^{-1}
U_{eq}	standard equilibrium potential, V
V	voltage, V
V_A	operating voltage, V
$W_{c,1}$	initial channel width, m
w_i	mass fraction of species i
w_j	mass fraction of species j
x_i	mole fraction of species i
x_j	mole fraction of species j
y_v	mole fraction of liquid water

Greek

α	charge transfer coefficient
δ_N	Nafion film thickness, m
δ_W	water film thickness, m

ε_N^{agg}	agglomerate-ionomer volume fraction, m^3 ionomer m^{-3} agglomerate
ε^v	void phase volume fraction
η	overpotential, V
μ	viscosity, Pa s
ξ	effectiveness factor
ρ	density, kg m^{-3}
σ_m	ionic conductivity, S m^{-1}
σ_s	electronic conductivity, S m^{-1}
τ	tortuosity
ϕ	potential, V
φ	Thiele modulus
ϕ_N	membrane phase potential, V
Ω	modeling domain

Superscripts and subscripts

0	intrinsic
a	anode
agg	agglomerate
c	cathode
CL	catalyst layer
eff	effective
eq	equilibrium
g	gas
GDL	gas diffusion layer
H_2	hydrogen
i	species i

j	species j
mem	membrane
N	Nafion®
N_2	nitrogen
O_2	oxygen
Pt	platinum
ref	reference
s	solid phase
v	void phase / vapor
w	liquid water